

# Symmetric Resonant Modes Between Twin Bodies

Robert K. M. Seah and Ronald W. Yeung

Department of Mechanical Engineering

University of California at Berkeley, Berkeley, CA 94720-1740, USA

E-mail: [robseah@yahoo.com](mailto:robseah@yahoo.com) & [rweyeung@berkeley.edu](mailto:rweyeung@berkeley.edu)

*With very best wishes to my good friend David Evans, on the occasion of his retirement. Professor Evans is an authority in linear water-wave theory, a field that he has very successfully explored and contributed to.* -R. W. Yeung

## 1 Introduction

When a moonpool is present between two bodies, its resonant motion introduces complex behavior of the water column and accordingly alters the hydrodynamic behavior of the surrounding bodies. Commonly studied resonances include the Helmholtz, or “pumping mode”, and other symmetric resonances. Antisymmetric modes, referred to as sloshing, are well known in its effects on motion of floating bodies. The latter have been addressed in several recent papers in the Workshop. One of the first studies of symmetric resonances was performed by Wang and Wahab (1971) who investigated the resonances of a moonpool between two semicircular floating bodies and noted the vanishingly small damping near the “zero-th” resonance mode. Miloh (1983) studied the wave load on a circular solar pond and noted similar behavior. Helmholtz modes also occur in closely related problems such as harbor resonance (Miles & Lee, 1974). More recently, Mavrakos (2004) studied the heave hydrodynamic coefficients for concentric cylinders of finite drafts.

McIver (1996) derived the streamlines of a twin body which does not radiate waves at infinity for a characteristic frequency. In essence, waves generated by the body only persist in the moonpool and local area near the bodies. This

created much interest in the so-called “trapped mode” resonance. Newman (1999) investigated the torodial form of the McIver streamline and Shipway and Evans (2003) studied the wave trapping behavior of concentric cylinders. Yeung and Seah (2004) investigated the effect of viscosity on the McIver streamlines. It was found that the time-domain solution of these shapes did not excite the oscillations at these trapped frequencies. In a number of common shapes like circular and rectangular cylinders, the Helmholtz mode of resonance reveals itself readily. This mode can be characterized by the absence of radiating waves but an appreciable amount of moonpool motion that is bounded.

In order to provide a better quantitative understanding of these Helmholtz modes and their modal shapes, the present study is directed to obtaining a semi-analytical solution of heaving twin rectangular cylinders. These results can also be obtained by an integral-equation formulation (say, Yeung, 1982) and other means, but the present analytical procedure is very accurate, and convergence of the solution is not an issue as the frequency approaches the Helmholtz and other resonance frequencies.

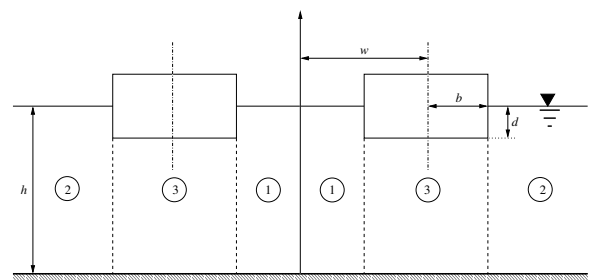


Figure 1: Schematic of the Fluid Domain.

## 2 Methodology

### 2.1 Division of solution domain

The approach used in this study is similar to that developed by Yeung (1981) and Fotsch (1997). Whereas the domains in these previous studies were subdivided into two subregions, the geometry here requires a subdivision effectively into three regions.

Figure 1 shows these regions as the inner moonpool water-column, exterior fluid domain and the fluid domain under the body. The distance from the axis of symmetry to the centerline of the bodies is denoted as  $w$  and each rectangular body has a half-beam of  $b$  and a draft of  $d$ . Water depth,  $h$ , is considered to be deep when  $h/d$  is greater than 20, for most wave-lengths. The fluid is taken to be inviscid and incompressible, with the amplitude of heave motion being small. Thus the velocity potential can be represented as:

$$\Phi(x, y, t) = \text{Re}[-i\sigma\zeta_2\phi(x, y)e^{-i\sigma t}] \quad (1)$$

where  $\sigma$  is the frequency of heave oscillation,  $\zeta_2$  is the heave amplitude. The spatial *unit* potential,  $\phi$ , takes a different functional form in each of the three subdomains and are denoted by  $\phi^{e1}$ ,  $\phi^{e2}$  and  $\phi^i$  for the moonpool, exterior and underbody regions, respectively. Each of these potentials are subject to a distinctive set of boundary conditions so the final form of  $\phi$  should be obtained by the matching of the potentials at the matching boundaries, ( $x = w \pm b$ , cf. Yeung, 1981). In the region under the body, the inhomogeneous boundary condition,

$$\frac{\partial\phi^i}{\partial y} = 1, \quad \text{at } y = -d, \quad (2)$$

is used to ‘drive’ the problem, resulting in the sum of a homogeneous ( $\phi^{ih}$ ) and a particular ( $\phi^{ip}$ ) solution.  $\phi^{ih}$  is an infinite set of eigenfunctions with eigenvalues satisfying

$$\gamma_n = \frac{n\pi}{h-d}, \quad n = 0, 1, \dots \quad (3)$$

giving the form of  $\phi^i$  as:

$$\phi^i = \phi^{ip} + \phi^{ih}. \quad (4)$$

It is easy to establish that

$$\phi^{ip} = \frac{1}{2(h-d)} \left[ (y+h)^2 - (x-w)^2 \right] \quad (5)$$

and

$$\phi^{ih} = \sum_{n=0}^{\infty} (C_{1n}X_{1n} + C_{2n}X_{2n})Y_n^i \quad (6)$$

$$X_{1n} = \begin{cases} 1 & \text{for } n = 0 \\ \frac{\cosh \gamma_n(x-w)}{\cosh \gamma_n b} & \text{for } n \geq 1 \end{cases} \quad (7)$$

$$X_{2n} = \begin{cases} x - w/b & \text{for } n = 0 \\ \frac{\sinh \gamma_n(x-w)}{\sinh \gamma_n b} & \text{for } n \geq 1 \end{cases} \quad (8)$$

$$Y_n^i = \begin{cases} 1 & \text{for } n = 0 \\ \cos \gamma_n(y+h)/\sqrt{\frac{1}{2}} & \text{for } n \geq 1. \end{cases} \quad (9)$$

$C_{1n}$  and  $C_{2n}$  are unknown coefficients to be determined from information in the other regions. Note that  $Y_n^i$  is a set of orthonormal functions such that the inner product can be defined as follows for any integer pair  $l$  and  $m$ :

$$\langle Y_l^i, Y_m^i \rangle \equiv \frac{1}{h-d} \int_{-h}^{-d} Y_l^i Y_m^i dy = \delta_{lm} \quad (10)$$

In a similar fashion, the linearized free-surface and bottom conditions for the remaining two regions result in another series of eigenfunctions with eigenvalues satisfying

$$m_0 \tanh m_0 h = \nu \quad (11)$$

$$m_k \tan m_k h = -\nu, \quad k = 1, \dots \quad (12)$$

where  $\nu = \sigma^2/g$ , the frequency parameter. Hence,  $\phi^{e1}$  and  $\phi^{e2}$  can be written in the form

$$\phi^q = \sum_{k=0}^{\infty} B_k^q \Lambda_k^q(x) Y_k^e(y) \quad (13)$$

where  $q = e1, e2$  and  $\Lambda_k^q, Y_k^e$  are defined as

$$\Lambda_k^{e1} = \begin{cases} \frac{\cos m_0 x}{\cos m_0(w-b)} & \text{for } k = 0 \\ \frac{\cosh m_k x}{\cosh m_k(w-b)} & \text{for } k \geq 1 \end{cases} \quad (14)$$

$$\Lambda_k^{e2} = \begin{cases} e^{im_0(x-(w+b))} & \text{for } k = 0 \\ e^{-m_k(x-(w+b))} & \text{for } k \geq 1 \end{cases}$$

and

$$Y_k^e = \begin{cases} \cosh m_0(y+h)/N_0^{1/2} & \text{for } k = 0 \\ \cos m_k(y+h)/N_k^{1/2} & \text{for } k \geq 1 \end{cases} \quad (15)$$

It should be noted that the expressions for  $\Lambda_k^{e1}$  exploits the symmetry property about the  $y$ -axis.  $B_k^q$  are another *two* new sets of unknown coefficients. The  $N_k$  are scale factors to achieve Eqn. (10) and are given by

$$N_k = \begin{cases} \frac{1}{2} \left[ 1 + \frac{\sinh 2m_0 h}{2m_0 h} \right] & \text{for } k = 0 \\ \frac{1}{2} \left[ 1 + \frac{\sin 2m_k h}{2m_k h} \right] & \text{for } k \geq 1 \end{cases} \quad (16)$$

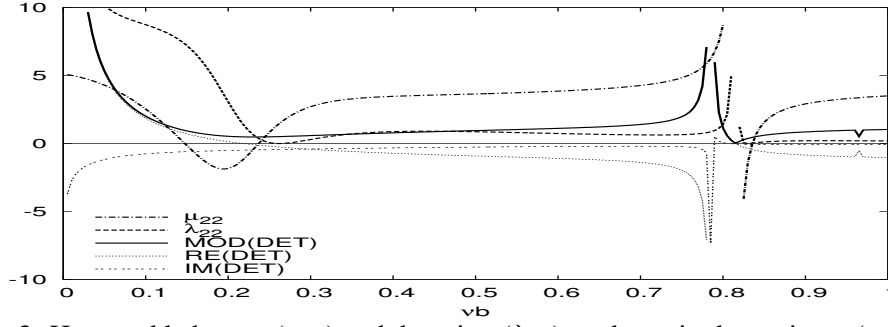


Figure 2: Heave added-mass ( $\mu_{22}$ ) and damping ( $\lambda_{22}$ ), and matrix determinant ( $w/b=5.0$ ).

## 2.2 Matching of solutions

To determine the values of  $C_{1n}$ ,  $C_{2n}$  and  $B_k^q$ , it is required that the potentials and fluxes be matched at  $x = w \pm b$ . These four matching conditions can be used so as to eliminate  $B_k^q$  from the equations, enabling  $\phi$  be entirely expressed in terms of  $C_{1n}$  and  $C_{2n}$ . Thus, a linear system of equations can be obtained,

$$\begin{aligned} & C_{1n} - C_{2n} - \\ & \frac{1}{h(h-d)} \sum_{k=0}^{\infty} \sum_{j=0}^{\infty} \frac{\Lambda_k^{e1}}{\Lambda_k^{e1r}} S_{kn} S_{kj} [C_{1j} X_{1j}' + C_{2j} X_{2j}'] \\ & = \frac{1}{h-d} \sum_{k=0}^{\infty} \frac{\Lambda_k^{e1}}{\Lambda_k^{e1r}} S_{kn} B_k^{e1*} - \langle \phi^{ip}, Y_n^i \rangle |_{x=w-b} \end{aligned} \quad (17)$$

$$\begin{aligned} & C_{1n} + C_{2n} - \\ & \frac{1}{h(h-d)} \sum_{k=0}^{\infty} \sum_{j=0}^{\infty} \frac{\Lambda_k^{e2}}{\Lambda_k^{e2r}} S_{kn} S_{kj} [C_{1j} X_{1j}' + C_{2j} X_{2j}'] \\ & = \frac{1}{h-d} \sum_{k=0}^{\infty} \frac{\Lambda_k^{e2}}{\Lambda_k^{e2r}} S_{kn} B_k^{e2*} - \langle \phi^{ip}, Y_n^i \rangle |_{x=w+b} \end{aligned} \quad (18)$$

where

$$S_{kn} = \begin{cases} \frac{\sinh m_0(h-d)}{m_0 N_0^{1/2}} & \text{for } k=0, n=0 \\ \frac{\sin m_k(h-d)}{m_k N_k^{1/2}} & \text{for } k \geq 1, n=0 \\ \frac{m_0(-1)^n \sinh m_0(h-d)}{\sqrt{\frac{1}{2}} N_0(m_0^2 + \gamma_n^2)} & \text{for } k=0, n \geq 1 \\ \frac{m_k(-1)^n \sin m_k(h-d)}{\sqrt{\frac{1}{2}} N_k(m_k^2 - \gamma_n^2)} & \text{for } k \geq 1, n \geq 1 \end{cases} \quad (19)$$

and

$$B_k^{q*} = \frac{1}{h} \int_{-h}^{-d} \phi_x^{ip} Y_k^e dy. \quad (20)$$

Terms on the RHS of Eqns. (17) and (18) are known and the \* is used to denote terms associated with the particular solution.

## 3 Illustrative Results and Discussions

The results presented here refer to a set of rectangular bodies with  $d/b = 1$  and  $w/b = 5$ . A depth-to-draft ratio,  $h/d$ , of 20 is taken to approximate deep water conditions. Figure 2 shows the heave hydrodynamic coefficients, non-dimensionalized by  $\rho b^2$ , and the determinant of the matrix formed by Eqns. (17) and (18). The frequency range

shown encompasses the Helmholtz frequency at  $(\nu b)_o = 0.263$  and the first symmetric resonance at  $(\nu b)_1 = 0.829$  as indicated by zero damping properties at these points. The indices of  $\nu b$  are assigned to the type of modes defined above.

With respect to these coefficients, it is interesting to note that the location of minimum (negative) added mass occurs before  $(\nu b)_o$ . In fact, it even precedes the location where the real component of the determinant vanishes. In contrast, at  $(\nu b)_1$ , both added mass and damping show singular behaviour preceding  $(\nu b)_1$ . In terms of the determinant, the two characteristic frequencies show differing behaviour as well. While a non-zero minimum in its absolute value is seen around  $(\nu b)_o$ , it clearly attains a zero absolute value for  $(\nu b)_1$ . Note that for the Helmholtz mode, though the coefficients vary rapidly around the Helmholtz frequency, they remain bounded.

Figure 3 are plots of the wave elevation in the moonpool region that are in-phase and out-of-phase with the body motion around  $(\nu b)_o$ . The in-phase component has a partial sinusoidal form with a negative mean value leading to the 'pumping or piston' nature of the resonance. However, while the form may be flattest at the fre-

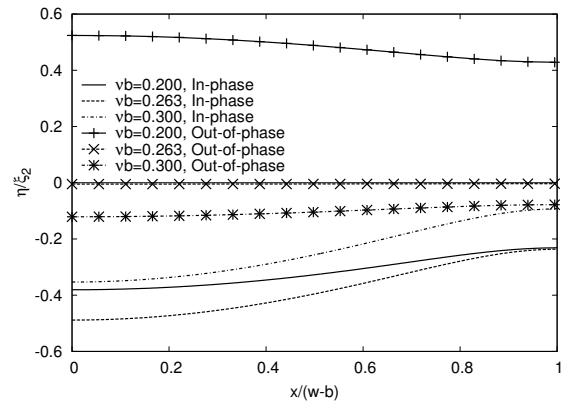


Figure 3: In- and Out-of-phase wave elevation around Helmholtz resonance.

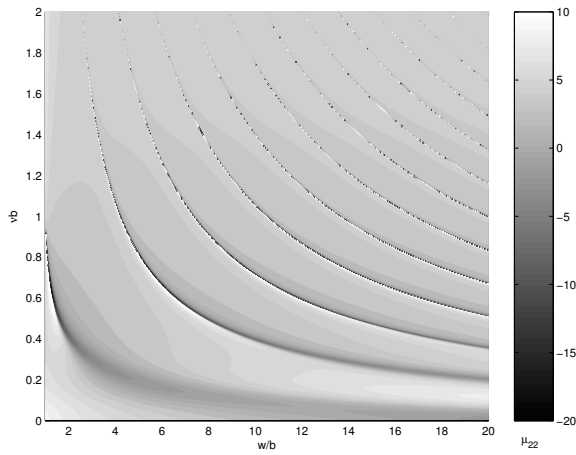


Figure 4: Variation of heave added mass with separation and frequency.

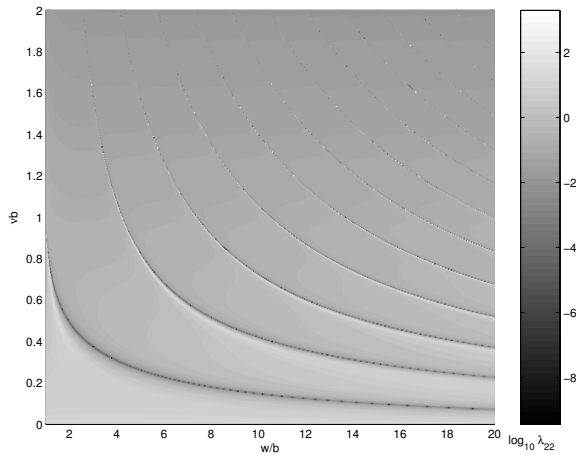


Figure 5: Variation of heave damping with separation and frequency.

quency of minimum added mass, the mean value appears to be most negative where the real component of the determinant crosses the zero value at  $\nu b = 0.232$ . Similarly, the out-of-phase component appears to have a partial sinusoidal form with a positive mean value, which decreases to be uniformly zero across the moonpool at  $(\nu b)_o$ . Beyond  $(\nu b)_o$ , it once again recovers its slightly sinusoidal form but with a negative mean value.

The effects of varying separation,  $w/b$ , can be seen in Figures 4 and 5 which are contour plots of the added mass and damping coefficients respectively. The lines clearly visible on these plots represent the loci of the resonances, with the bottom line being the loci of the Helmholtz frequencies  $(\nu b)_o$  and the rest being the higher frequency symmetric resonances.

An interesting feature is that  $(\nu b)_o$  approaches a finite value as the moonpool becomes infinitely small which is in contrast to the rest of the dark

lines as they approaches infinity. Also, the clearly singular behaviour at the  $(\nu b)_n$ ,  $n > 0$ , frequencies can be seen as a sharp switchover from black to white in the contour plot. Examining the loci of  $(\nu b)_o$  in Figure 4, the Helmholtz resonance appears to manifest initially as having very spiky behaviour which quickly softens to a modest local minimum as seen in Figure 2. As frequency increases, Helmholtz resonance becomes indistinct. Figure 5 is plotted in logarithmic scale, facilitating the identification of the loci of  $(\nu b)_o$ . This loci appears to tend to smaller frequencies as separation increases, as with all the other resonant modes.

The results here show the effects of frequency and separation on the behaviour of the moonpool resonances. However, many other parameters, like draft variation, can also effect its behavior. Thus, further results will be presented at the workshop.

## References

- [1] A.R. Fotsch, Graduate Student Paper, *SNAME, Nor-Cal Section*, April 10, 1997, 31 pp.
- [2] S.A. Mavrakos, *Appl. Ocean Res.* 26 (2004) 84–97.
- [3] M. McIver, *J. Fluid Mech.* 315 (1996) 257–266.
- [4] J.W. Miles and Y.K. Lee, *J. Fluid Mech.* 67 (1975) 445–464.
- [5] T. Miloh, *Proc. Int'l Workshop on Ship and Platform Motions*, University of California, Berkeley (1983) pp.110–131.
- [6] J.N. Newman, *J. Engrg. Math.* 35 (1999) 135–147.
- [7] B.J. Shipway and D.V. Evans, *J. Offshore Mech. and Artic Engrg.* 125 (2003) 59–64.
- [8] S. Wang and R. Wahab, *J. Ship Research* 15, No.1 (1971) 33–48.
- [9] R.W. Yeung, *Appl. Ocean Res.* 3, No.3 (1981) 119–133.
- [10] R.W. Yeung, *Memorandum of Computational Hydrodynamics Laboratory*, Mass. Inst. of Tech., Cambridge, MA, (1982) 5 pp.
- [11] R.W. Yeung and R.K.M. Seah, *Proc. 19th Int'l Workshop on Water Waves and Floating Bodies*, Cortona, Italy (2004).